Abdominal Radiology

Published online: 18 September 2018

Abdom Radiol (2019) 44:723–731
https://doi.org/10.1007/s00261-018-1771-1

Hypoenhancing prostate cancers on dynamic contrast-enhanced MRI are associated with poor outcomes in high-risk patients: results of a hypothesis generating study

V. F. Muglia,[1,7] R. B. Reis,[2] T. O. Rocha,[3] A. R. Silva,[4] S. Noworolski,[5] and A. C. Westphalen[6]

[1]Radiology Division, Department of Internal Medicine, Ribeirão Preto School of Medicine, University of São Paulo, Ribeirao Preto, SP, Brazil
[2]Urology Division, Department of Surgery, Ribeirão Preto School of Medicine, University of São Paulo, Ribeirao Preto, SP, Brazil
[3]Ribeirão Preto School of Medicine, University of São Paulo, Ribeirao Preto, SP, Brazil
[4]Department of Pathology, Ribeirão Preto School of Medicine, University of São Paulo, Ribeirao Preto, SP, Brazil
[5]Department of Radiology and Biomedical Imaging, School of Medicine, University of California at San Francisco, San Francisco, USA
[6]Departments of Radiology and Biomedical Imaging, and Urology, School of Medicine, University of California at San Francisco, San Francisco, USA
[7]Hospital de Clínicas, Ribeirão Preto School of Medicine, University of São Paulo (USP), Av Bandeirantes 3900, Campus Monte Alegre, Ribeirao Preto, SP 14049-900, Brazil

Abstract

Purpose: To investigate the association of hypoenhancement on dynamic Contrast enhanced (DCE) with prostate cancer patient outcomes.
Material and methods: This was a single-institution retrospective Institutional Review Board (IRB)-approved cohort study of 54 men who had prostate Magnetic Resonance Imaging (MRI) within 6 months of cancer diagnosis between 01/2012 to 03/2014. Two readers independently identified the dominant MRI-lesions utilizing Prostate Imaging—Reporting and Data System-version2- guidelines. These lesions were classified as hypoenhancing or hyperenhancing, compared to normal peripheral zone using quantitative DCE analysis. The *t* test for unequal sample sizes and the two-sample Wilcoxon rank-sum tests were used to compare groups. Logistic regression determined if DCE characteristics predict the development of metastases or prostate cancer death.
Results: Time-to-progression was significantly shorter for hypoenhancing tumors (6.2 vs. 24.8 months, $p = 0.05$). Men with these lesions had a higher odds of having poor outcome (univariate logistic regression, odds ratio (OR) 6.79, 95% confidence interval (CI) 1.45–31.72, $p = 0.02$; multivariate analysis, OR 2.05, 95% CI 0.30–13.72, $p = 0.47$). Hypoenhancing tumors were larger (33.1 vs. 19.1 mm, $p < 0.001$) and more likely to be intermediate (Gleason scores 3 + 4 and 4 + 3) and high-grade (Gleason scores ≥ 4 + 4) prostate cancers ($p = 0.05$). Men in the hypoenhancing group had a higher mean prostate-specific antigen (PSA) value (87.6 vs. 24.8 ng/dL, $p = 0.01$) and PSA density (1.54 vs. 0.72, $p = 0.03$). The mean K_{trans} and k_{ep} of hypoenhancing lesion were lower when compared to hyperenhancing lesions ($p = 0.03$ and $p = 0.04$). V_e values did not differ ($p = 0.25$).
Conclusion: Men with hypoenhancing prostate cancers may have a worse prognosis than men with hyperenhancing tumors.

Key words: Prostate cancer—Magnetic resonance imaging—Diffusion MRI—Perfusion—Hypoxia

Magnetic resonance imaging (MRI) has emerged as an important tool for the assessment of prostate cancer, being used for detection, staging, characterization of

Correspondence to: V. F. Muglia; *email:* fmuglia@fmrp.usp.br

aggressiveness, and relapse after treatment [1]. Recently, following the publication of the second version of the prostate imaging—reporting and data system (PI-RADS) guidelines, the acquisition protocol underwent significant standardization [2]. Now, DCE is described as positive when early or contemporaneous enhancement to adjacent tissue is identified, i.e., when the tumor is iso or hyperenhancing, and negative otherwise.

The use of dynamic contrast-enhanced (DCE) is controversial, though. Some authors recommend excluding it to simplify and streamline the prostate MRI protocol [3–5], while its proponents say prostate cancer is typically a hyperenhancing lesion compared to normal peripheral zone (PZ) and that this feature can be used to predict histologic grade and tumor aggressiveness [6–11].

Some prostate cancers are not hyperenhancing, and compared to other types of cancer [12–14], there is limited research on the prevalence and significance [15] of prostate cancers with this enhancement pattern. Hypoenhancing cervical cancers, for example, have been associated with a worse prognosis, manifested by inadequate local control, high rate of local recurrence, and systemic dissemination [16, 17]. Furthermore, Loncaster et al [16] were able to correlate the pattern of perfusion on DCE MRI with tumor hypoxia, which is an independent predictor of poor prognosis in cervical and prostate cancer [18–20]. Only a few imaging studies have investigated the effect of hypoxia on the biological behavior of prostate cancer using DCE MRI and blood oxygenation level dependence (BOLD) [21, 22].

As PI-RADS v2 only considers DCE MRI as positive when enhancement is high, it is possible that some aggressive cancers will be underestimated. Accordingly, we conducted this preliminary retrospective cohort study to investigate the association of hypoenhancement on DCE with prostate cancer patient outcomes.

Material and methods

Patients selection

This single-institution retrospective study was approved by our IRB with a waiver of signed informed consent. Men who underwent multiparametric MRI of the prostate within 6 months prior to histological confirmation of prostate cancer and had a minimum follow-up time of 36 months were eligible for inclusion. Scans were acquired between January 2012 to March 2014. A total of 158 patients were initially identified, but 36 were excluded because of previous treatment (prostatectomy $n = 21$ and radiation therapy plus/minus androgen deprivation therapy $n = 15$), 22 because intravenous contrast media was not used or images were suboptimal limiting analysis (e.g., contrast leakage), and 18 due to loss to follow-up.

Furthermore, patients were only included in the study if a lesion was visible to both readers, and it was classified as PI-RADS 4 or 5 by at least one of them. A visible lesion was defined as a PI-RADS v2 score ≥ 3. In other words, at the very least, a lesion had to be classified as a PI-RADS v2 3 lesion by one reader and PI-RADS v2 4 by the other. After MRI qualitative analysis (see below), 28 patients had no visible lesions or lesions that were visible but classified as indeterminate (PI-RADS v2 = 3) by both observers and were, therefore, excluded. Accordingly, after applying all criteria, 54 patients were included in this study. The flowchart, with respective exclusions, is seen on Fig. 1.

MRI protocol

MR imaging was performed with a 1.5 T scanner (Achieva, Philips, Best, Netherlands) using a pelvic phased-array and an endorectal coil simultaneously activated. The protocol included high-resolution axial, coronal, and sagittal T2-weighted imaging, diffusion-weighted imaging (DWI), and DCE MRI. T2-weighted imaging and DWI were acquired before the administration of contrast. DWI was acquired with *b*-values of 0, 250, 500, and 1000 s/mm^2 and with an inline reconstruction of apparent diffusion coefficient (ADC) map. DCE MRI was performed after administration of 0.1 mmol of gadopentetatedimeglumine (Magnevist, Bayer HealthCare) per kilogram of body weight, followed by a 20-mL saline flush at a rate of 3 mL/s. The temporal resolution was set between 6 and 8 s. The complete protocol is given in Table 1.

MRI qualitative analysis

MRI qualitative analyses were independently performed by two observers, blinded to the clinical and pathological data, but aware that all patients had prostate cancer, both readers had more than 10 years of experience in

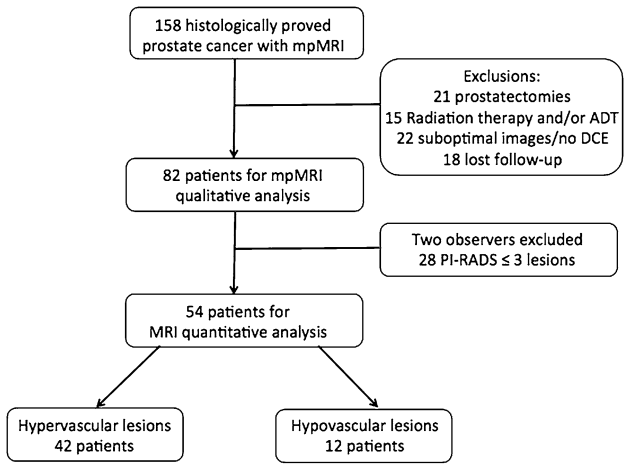

Fig. 1. Flowchart showing patient recruitment and exclusions.

Table 1. MRI sequences and respective parameters

Sequence	Technique	TR/TE (ms)	Flip° (degrees)	Slice thickness (mm)	FOV (mm)	Matrix
T2WI						
Axial	TSE	3060/100	90	3	150 × 150	232 × 184
Coronal	TSE	2444/120	90	3	150 × 150	248 × 198
Sagittal	TSE	3770/120	90	3	260 × 260	360 × 275
DWI*						
Axial	SE EPI	1561/71	90	5	304 × 375	152 × 152
DCE‡						
Axial	THRIVE	4/2	10	4	297 × 345	172 × 172
T1WI						
Axial	TSE	443/15	90	3	180 × 180	180 × 143

Number of average is 2 for all sequences, except for DCE (THRIVE), which is one
T2WI, T2 weighted imaging; DWI, diffusion-weighted imaging; DCE, dynamic contrast material–enhanced imaging; T1WI, T1 weighted imaging; TR, repetition time; TE, echo time; Flip°, flip angle; FOV, field of view; TSE, turbo spin echo; SE EPI, spin-echo echo-planar imaging; THRIVE, T1 high-resolution isotropic volume excitation
*b values were 0 and 1000 s/mm^2
‡The section thickness was 4 mm with interpolated into 2 mm on DCE MR image

prostate imaging (—, —) and used a commercially available workstation (Philips, Best, Netherlands). Readers independently analyzed T2-weighted, DWI, and DCE images from all patients and classified findings according to the PI-RADS v.2 guidelines. Readers were asked to identify the dominant lesion. Index lesions was defined as the one with high PI-RADS score and tie-brake rule was size of the lesion on most visible sequence, T2 or ADC. Measurement of the longest axis and mean ADC value of the index lesions were recorded. Lesions were located according to the scheme proposed by PI-RADS [4] to facilitate correlation between readers.

DCE MRI quantitative analysis

Four months after the qualitative evaluation, one of previous observers (—), performed the quantitative analysis of all consensual visible lesions (n = 54) using Osirix software, version 7.3 (Pixmeo, Geneve, Switzerland) and the DCE Tool Plugin, developed at University of California at Los Angeles and previously tested in other studies [23, 24]. Regions-of-interest (ROI) were drawn on the common femoral artery, on the prostate cancer index lesions, using T2-weighted images and ADC maps as reference (Fig. 2), and on the contralateral normal peripheral zone. The ROIs that were drawn on the lesions had an area of at least 10 mm^2; and one ROI was drawn on each slice that showed the lesion. Accordingly, multiple time-intensity curves were generated for each lesion. Curve types were classified as: type 1, when progressive enhancement was seen throughout the acquisition; type 2, when rapid signal elevation was followed by a plateau; and type 3, when rapid signal elevation was followed by wash out. Three approaches were used for quantitative analyses of lesion enhancement. First, lesions were divided into two groups, hyperenhancing or hypoenhancing. Hyperenhancing lesions were those lesions in which the predominant signal intensity was equal to or greater than the adjacent normal area of peripheral zone, and hypoenhancing lesions were those with a predominant signal intensity that was at least 10% lower than the adjacent normal peripheral zone, a concept derived from breast cancer DCE analysis [25]. Figures 3 and 4 show examples of a hyper and of a

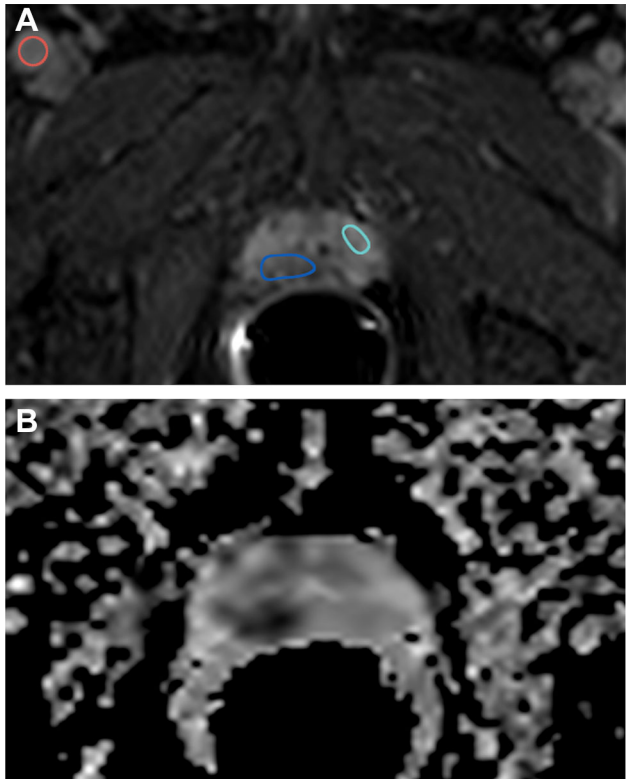

Fig. 2. ROI placement pattern for quantitative analyses of DCE. ROIs were drawn on the common femoral artery, normal peripheral zone, and index lesion (**A**) utilizing the information seen the ADC map image (**B**).

hypoenhancing tumor. Second, a slope angle was calculated based on average signal intensity variation in the first 30 seconds from peak intensity in the external iliac artery. Third, a pharmacokinetic analysis was performed according to the multicompartimental exchange model described by Tofts and Kermode [26], where the contrast agent is distributed in intra and extracellular spaces. Two independent parameters were evaluated using the Tofts–Kermode model, K_{trans} and k_{ep}. We also assessed the total extracellular extravascular space (EES) volume ($V_e = K_{trans}/k_{ep}$). For the K_{trans} and k_{ep} measurements, T1 mapping was obtaining by using multiple variable flip angle (VFA) and the modified Fritz-Hansen technique for artery input function (AIF).

Transrectal ultrasound (TRUS)-guided biopsy

Biopsy was performed using a Logiq E9 scanner, manufactured by General Electric, Milwaukee, using an extended sextant technique. Four staff radiologists, all with more than 4 years of prostate biopsy experience, performed or supervised the procedures. MRI data were available at the time of the procedure for consultation, and all biopsies were performed using a cognitive approach to correlate TRUS and MRI. At least twelve core samples were obtained from all patients, but for some men up to 20 fragments were collected. In all but two cases the lesions that were described on MRI were reported to be visible on TRUS.

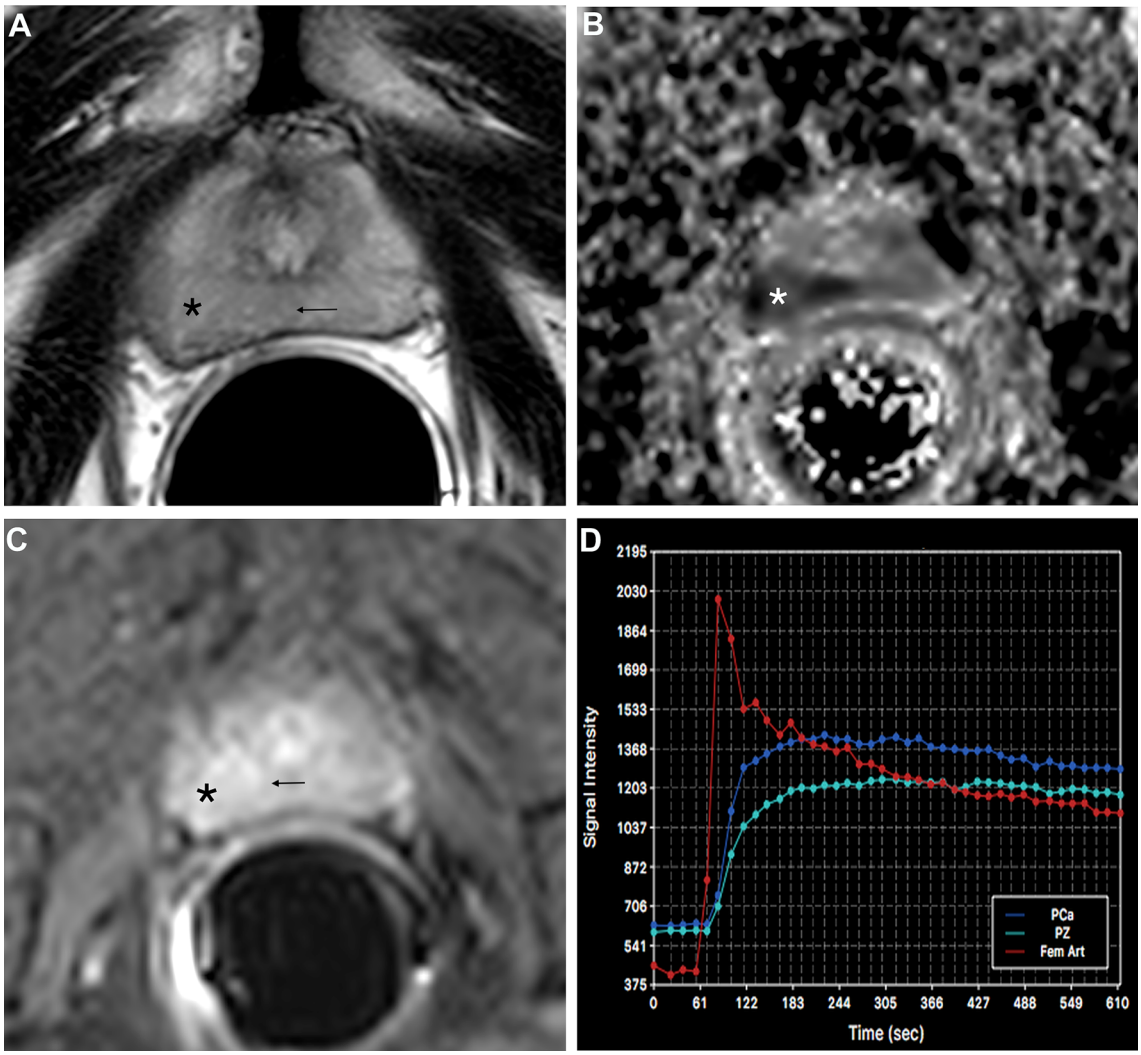

Fig. 3. Hypervascular lesion. 75-year-old man, PSA = 25.7 ng/mL. T2-weigthed image showing a subtle low signal intensity lesion in the right apex and midgland (asterisk and arrow on **A**). The ADC map clearly shows the lesion, which has a mean ADC value of 0.965×10^{-3} mm/s^2 (**B**). Post-contrast T1-weigthed image shows a hypervascular lesion (asterisk and arrow on **C**); and the time-intensity curve (**D**) confirms its hypervascular nature. After surgery, a Gleason 3 + 4 prostate cancer was confirmed. The patient died 39 months later due to complications of pulmonary fibrosis.

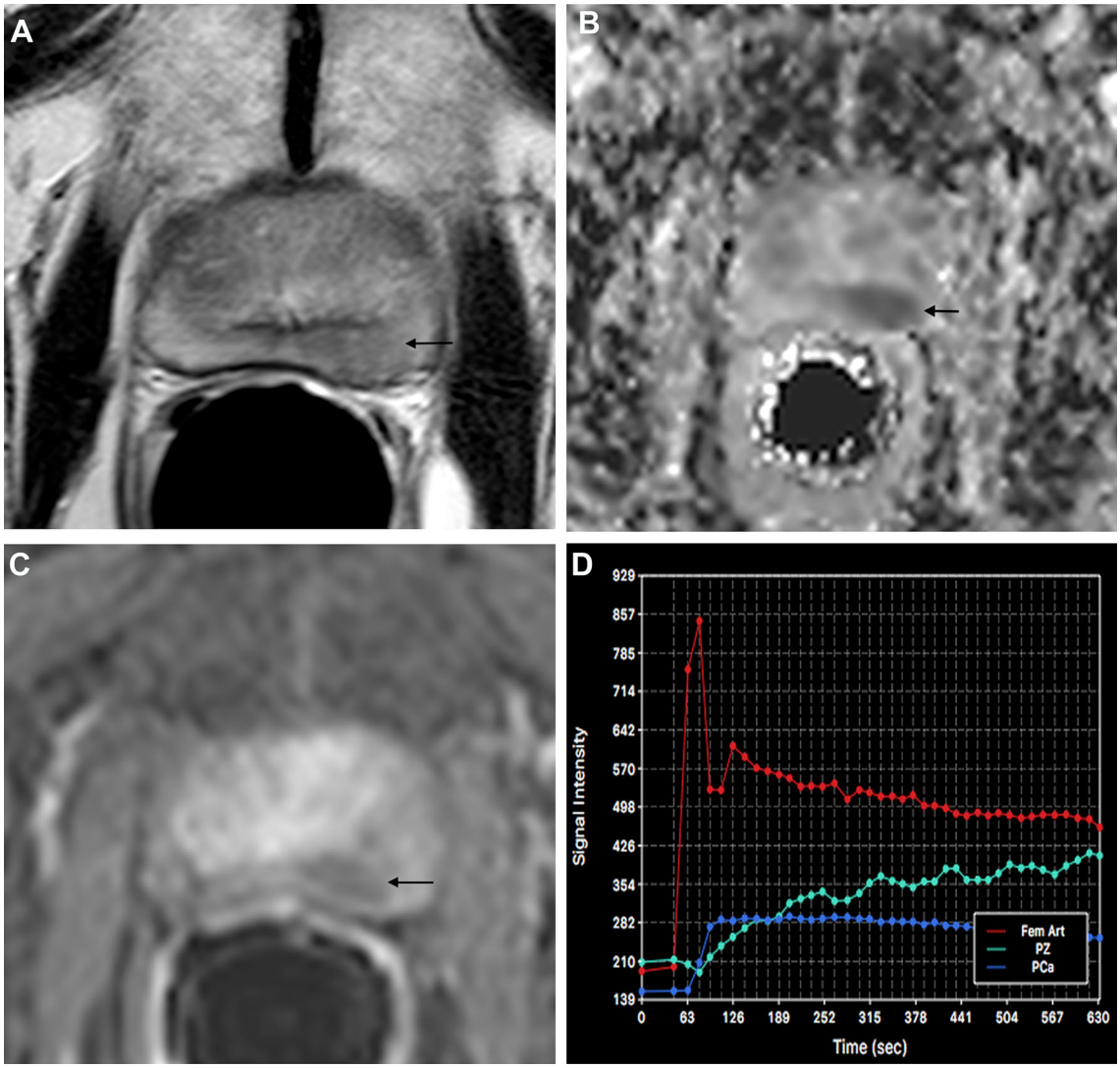

Fig. 4. Hypovascular lesion. 83-year-old man, PSA = 10.6 ng/mL. T2-weigthed image showing a lesion with markedly low signal intensity in the left apex (arrow on **A**). The ADC map clearly shows the lesion, which has a mean ADC of value of 0.993×10^{-3} mm/s^2 (arrow on **B**). Post-contrast T1-weigthed image shows a hypovascular lesion (arrow on **C**); and time-intensity curve (**D**) confirms the hypovascularity of the lesion (K_{trans} = 0.0705 and k_{ep} = 0.1901). After surgery, a Gleason 4 + 4 prostate cancer was confirmed. The patient presented with biochemical failure and developed metastases 26 months later.

Histopathological analysis

All biopsy samples were routinely fixed in 4% neutral formalin and embedded in paraffin. Samples were stained with hematoxylin-eosin and immunohistochemistry, as necessary. A dedicated uropathologist (—) with more than 15 years of experience in the field reviewed all specimens. Primary and secondary Gleason were recorded for all lesions.

Outcomes

All demographic and clinical data, including therapeutic choice, patient outcomes (systemic recurrence, documented by imaging and/or biopsy, or disease-related death), and time to any event in outcome (systemic metastasis or death), were reviewed. Therapeutic choices were made according to Urology International Guidelines and patient's desire, varying from radical prostatectomy, radiation therapy, alone or in combination with androgen deprivation therapy (ADT), ADT alone, and active surveillance.

Statistical analysis

The dominant lesion was the unit of analyses. We used logistic regression models to determine the predictors of development of metastates or death. Models were built using both a forward and a backward approach [23]. The

following variables were considered for inclusion in the models alongside DCE characteristic: total serum PSA, PSA density, Gleason score, International Society of Uropathology (ISUP) group, tumor stage, tumor size, ADC mean value, and treatment. Tumor size was the only variable selected for inclusion using both the forward and backward approaches. We also utilized the *t* test for unequal sample sizes, Pearson's chi-square, and the two-sample Wilcoxon rank-sum (Mann–Whitney) test to compare other characteristics of patients and tumors. The average of both readers measurements of lesion size and ADC values was utilized in the analyses. All analyses were performed using Stata version 13.1 (College Station, TX). p values < 0.05 were considered statistically significant.

Results

Of 82 histologically proven cancers, reader 1 recorded 62 visible lesions, i.e., PI-RADS ≥ 3 (62/82, 75.6%), while reader 2 recorded 61 lesions (61/82, 74.4%). Fifty-four patients had coincident visible lesions classified as PI-RADS 4 or 5 by at least one of the readers and, therefore, were selected for quantitative analysis. The distribution of assigned PI-RADS scores is shown in Table 2.

First, forty-two lesions were classified as hyperenhancing (42/54, 77.8%) and 12 as hypoenhancing (12/54, 22.2%).

The mean age of men was 67.8 ± 6.8 years, without a difference between groups ($p = 0.40$).

The time-to-progression (TTP) to metastases or death was shorter for hypoenhancing tumors, 6.2 ± 5.2 months, compared to hyperenhancing ones, 24.8 ± 6.1 months ($p = 0.05$). Logistic regression shows that a patient with a hypoenhancing lesion is more likely to develop metastases or die of prostate cancer than men with hyperenhancing lesions, though the result was only statistically significant on the univariate analysis. On univariate analysis, the odds of developing metastases or dying of prostate cancer were over 6 times higher in men with hypoenhancing tumors (OR 6.79, 95% CI 1.45–31.72, $p = 0.02$). In addition to the enhancement characteristics, the multivariate model included tumor size, PSA, and PSAD, the only variables shown to be an independent predictors based on backward and forward selection. In this model the odds of developing metastases or dying of prostate cancer were about two and half times higher in men with hypoenhancing tumors (OR 2.53, 95% CI 0.26–24.42, $p = 0.43$). In both models the 95% CIs show that most results of repeated experiments are likely to fall clearly above the 1.0 threshold of significance. These results are summarized in Table 3.

The mean PSA and PSA density values, size, and Gleason/ISUP scores of hypoenhancing tumors were higher than hyperenhancing ones. Clinical and demographic data are shown in Table 4.

Analyses of the type of enhancement showed no difference in their distribution, with a predominance of type 2 curve (plateau) for both groups ($p = 0.33$).

Similarly, the slope angle of enhancing did not differ significantly. The slope angle of hyperenhancing lesions was 65.3 ± 1.29 degrees and of hypoenhancing lesions, 60.3 ± 3.5 degrees ($p = 0.10$).

K_{trans} and k_{ep} values were statistically different between groups. The mean K_{trans} value of hyperenhancing lesions was 0.0838 ± 0.0097 mL/g/min, and 0.0415 ± 0.0055 mL/g/min for hypoenhancing lesions, $p = 0.03$. And the mean k_{ep} of hyperenhancing lesions was $0.1775 \pm 0.027\ min^{-1}$, compared to $0.0679 \pm 0.017\ min^{-1}$ for hypoenhancing lesions ($p = 0.04$). The total EES volume (V_e) was not statistically different between the two groups, 0.6343 ± .0304 mL/g for hyperenhancing and 0.7209 ± .0662 mL/g for hypoenhancing group ($p = 0.25$).

There was no statically significant difference of the mean ADC value between the two groups. The mean ADC values were $0.927 \pm 0.164 \times 10^{-3}\ mm/s^2$ and $0.858 \pm 0.152 \times 10^{-3}\ mm/s^2$ for hyperenhancing and hypoenhancing tumors, respectively ($p = 0.20$). All DCE and DWI results are shown in Table 5.

Table 2. Distribution of coincident visible lesions (PI-RADS ≥ 3) classified as PI-RADS 4 or 5 by at least one of the readers

	Reader 2			
PI-RADS score	3	4	5	Total
Reader 1				
3	–	1	–	1
4	2	8	6	16
5	–	2	35	37
Total	2	11	41	54

PI-RADS, prostate imaging reporting and data system

Table 3. Univariate and multivariate logistic regressions

	Odds ratio	*P* value	95% CI
Univariate			
DCE characteristic	6.79	0.02	1.45–31.72
Multivariate			
Size (mm)	1.17	0.007	1.04–1.30
PSA	0.96	0.03	0.93–0.99
PSAD	7.91	0.02	1.44–43.54
DCE characteristic	2.52	0.42	0.26–24.43

mm, millimeters; PSA, prostate-specific antigen; PSAD, prostate-specific antigen density; DCE, dynamic contrast enhanced; CI, confidence interval

Table 4. Demographic, clinical, pathologic data by DCE characteristics

	Hyperenhancing $n = 42$	Hypoenhancing $n = 12$	P value
Age (years)	67.4 ± 6.8	69.3 ± 7.1	0.40
PSA (ng/dL)	24.8 ± 33.9	87.6 ± 143.9	0.01
Lesion size (cm)	1.98 ± 0.77	3.31 ± 1.39	0.0001
Follow up (months)	36.9 ± 5.8	35.6 ± 10.9	0.58
Time-to-progression (months)	24.8 ± 6.1	6.2 ± 5.2	0.05
Gleason (ISUP groups)			
3 + 3 (group 1)	4 (9.8%)	1 (8.3.%)	0.07 (0.05†)
3 + 4 (group 2)	10 (24.4%)	0 (0%)	
4 + 3 (group 3)	12 (29.3%)	2 (16.7%)	
4 + 4 (group 4)	8 (19.5%)	4 (33.3%)	
4 + 5 (group 5)	2 (4.9%)	2 (16.7%)	
5 + 4 (group 5)	2 (4.9%)	2 (16.7%)	
5 + 5 (group 5)	3 (7.3%)	0 (0%)	
Clinical staging			
T2a	11 (26.2%)	4 (33.3%)	0.21
T2b	9 (21.4%)	0 (0%)	
T2c	13 (31.0%)	2 (16.7%)	
T3a	5 (12.0%)	6 (50.0%)	
T3b	1 (4.2%)	0 (0%)	
Treatment			
Prostatectomy	22 (52.4%)	3 (25.0%)	0.008 (0.22*)
Radiation therapy	15 (35.7%)	6 (50.0%	
Radiation therapy + ADT	4 (9.5%)	0 (0%)	
ADT	0 (0%)	3 (25.0%)	
Watchful waiting	1 (2.4%)	0 (0%)	

DCE, dynamic contrast enhanced; PSA, prostate-specific antigen; ISUP, International Society of Urological Pathology; ADT, androgen deprivation therapy
†Number is parenthesis refers to ISUP analysis
*Excluding 4 patients who received only ADT or was under watchful waiting

Table 5. DCE and DWI parameters by DCE characteristics

	Hyperenhancing $n = 42$	Hypoenhancing $n = 12$	P value
Slope (degrees)	65.2 ± 8.3	60.3 ± 12.2	0.10
K_{trans} (mL/g/min)	0.0838 ± 0.0097	0.0415 ± 0.0193	0.03
k_{ep} (min^{-1})	0.1775 ± 0.1793	0.0679 ± 0.0591	0.04
V_e (mL/g)	0.6343 ± .0304	0.7209 ± .0662	0.47
Type of curve			
1	01 (02.4%)	–	0.33
2	31 (73.8%)	11 (91.7%)	
3	10 (23.8%)	01 (08.3%)	
Mean ADC ($\times 10^{-3}$ mm/s^2)	0.924 ± 0.163	0.858 ± 0.152	0.21

DCE, dynamic contrast enhanced; DWI, diffusion weighted imaging; K_{trans}, volume transfer constant; k_{ep}, flux rate constant; V_e, volume of the extravascular extracellular space; ADC, apparent diffusion coefficient

Discussion

The results of this study demonstrate an association between hypoenhancement on DCE MRI and several other features that have been shown to be indicative of biologically aggressive disease and worse prognosis (high serum PSA, large tumor size, and high Gleason score). This aggressive behavior was seen in spite of lesions having been assigned the same PI-RADS v2 scores as less aggressive lesions. Furthermore, men with hypoenhancing lesions progressed earlier and were more likely to develop metastases or to die of prostate cancer. This suggests DCE findings have a prognostic role when assessing men with prostate cancers.

Although the results cannot be extrapolated to men with low-risk prostate cancer, these findings are particularly important in light of recent studies that have suggested a simplified MRI protocol for prostate cancer evaluation based only on T2 and DWI images [3–5]. Furthermore, the recently released PI-RADS [2] determines that DWI and T2-weighted images are considered the main sequences for the assessment of prostate cancer,

giving DCE only a secondary role for the evaluation of lesions located in the peripheral zone.

The use of DCE in the setting of prostate cancer has been investigated [10, 11] and the usual patterns seen within the peripheral and transition zones, well defined [6]. Tumors are usually hyperenhancing when compared to normal peripheral zone tissue [3, 6–9] and most frequently demonstrate a type 2 enhancement curve (plateau, i.e., rapid elevation followed by constant signal intensity) or, the most specific pattern, the type 3 (''wash in/wash out'') curve, which has also been associated with many other cancers, e.g., breast cancer [24]. Yet, a hypoenhancing pattern on DCE is recognized in some forms of cancer as a predictor of poor outcomes, for example cervical cancer [16, 17]. Although data is scarce, it has been suggested that high-grade prostate cancers exhibit lower enhancement than low or intermediate-grade cancers. In the model we have used, Dynamic relaxivity contrast-enhanced MRI, with kinetic parameters like transfer constants and extracellular space, these alterations have been related to smaller acinar glands and thus, higher cell density [18, 27], and expression of angiogenic cytokines as vascular endothelial growth factor (VEGF) [28]. While this hypoenhancing pattern has been attributed to hypoxia, this has been investigated but not clinically validated in vivo, although combined MRI approach focusing on perfusion and diffusion techniques are currently under investigation [21, 29]

While on multivariate analysis the enhancement characteristics of the tumors was not an independent predictor of metastases or death, the range and distribution of values within the 95% CI suggests that men with a hypoenhancing lesion have higher odds of developing these adverse outcomes. The wide 95% CI is a result of the small sample size. It is also interesting to note that a hypoenhancing pattern improved the prediction of outcomes even among tumors with markedly low mean ADC values, a feature that has been established as an independent predictor of poor prognosis [30].

This study has limitations. Given its retrospective nature, it is prone to selection bias. Because we restricted the study to the period during which we utilized a state-of-art DCE protocol, as recommended by the European Society of Uroradiology in 2012 [31] and the current PI-RADS guidelines [2], and included only patients who had sufficient follow-up, the sample size is not large. The high prevalence of high-grade tumors in this series limits generalizability. This prevalence of high-grade cancers may be related to the referral pattern to this public tertiary hospital, where there is a predominance of patients from low socioeconomic levels, who disproportionately do not undergo screening. A cognitive approach to the correlation between TRUS and MRI was utilized, rather than TRUS-MRI fusion or in-bore MR-guided biopsy. Yet, most lesions were visible during TRUS, MRI images were available at the time of the procedures, and lesions were large, mitigating the limitations of cognitive correlation between the imaging modalities. Diffusion-weighted MR images were generated from a 1000 s/mm^2 *b* value acquisition, while PI-RADS v2 recommends a *b*-value of at least 1400 s/mm^2. Yet, this is a recommendation, rather than an absolute rule and a *b*-value of 1000 s/mm is accepted in PI-RADS v2. The result of using a slightly lower *b*-value is lower contrast between cancer and normal tissue on DWI signal intensity, but not on the ADC map. Theoretically this could result in a tendency to underestimate the PI-RADS score of lesions located in the peripheral zone; however, there is no reason to believe this is a systematic bias and if we did exclude lesions based on the DWI findings, we equally impacted hyperenhancing or hypoenhancing lesions.

In conclusion, our study shows that men with hypoenhancing prostate cancers may have a worse prognosis than men with hyperenhancing tumors.

Compliance with ethical standards

Conflict of interest V.F. Muglia, R.B. Reis, T.O. Rocha, A.R. Silva, and S. Noworolski declares no conflict of interest. A.C. Westphalen is member of Scientific Advisory Board of 3D Biopsy, LLC.

Ethical approval All procedures performed in this study, involving human participants, were in accordance with the ethical standards of the Institutional Review Board and with the 1964 Helsinki declaration and its later amendments or comparable ethical standards. The study was approved by our IRB with a waiver of signed informed consent.

References

1. Fulgham PF, Rukstalis DB, Turkbey IB, et al. (2017) AUA standard operating procedure for MRI of the prostate. J Urol 198:832–838
2. ACR. MR prostate imaging reporting and data system version 2.0. Washington, DC: American College of Radiology; 2015 [updated 2015; cited 2015 04/16]. http://www.acr.org/Quality-Safety/Resources/PIRADS/
3. Rais-Bahrami S, Siddiqui MM, Vourganti S, et al. (2015) Diagnostic value of biparametric magnetic resonance imaging (MRI) as an adjunct to prostate-specific antigen (PSA)-based detection of prostate cancer in men without prior biopsies. BJU Int 115(3):381–388
4. Stanzione A, Imbriaco M, Cocozza S, et al. (2016) Biparametric 3T magentic resonance imaging for prostatic cancer detection in a biopsy-naive patient population: a further improvement of PI-RADS v2? Eur J Radiol 85(12):2269–2274
5. Stanzione A, Imbriaco M, Cocozza S, et al. (2017) Erratum to ''Biparametric 3t magnetic resonance imaging for prostatic cancer detection in a biopsy-naive patient population: a further improvement of PI-RADS v2? [Eur. J. Radiol. 85 (12) (2016) 2269-2274]''. Eur J Radiol 87:125
6. Ren J, Huan Y, Wang H, et al. (2008) Dynamic contrast-enhanced MRI of benign prostatic hyperplasia and prostatic carcinoma: correlation with angiogenesis. Clin Radiol 63(2):153–159
7. Franiel T, Hamm B, Hricak H (2011) Dynamic contrast-enhanced magnetic resonance imaging and pharmacokinetic models in prostate cancer. Eur Radiol 21(3):616–626
8. Oto A, Yang C, Kayhan A, et al. (2011) Diffusion-weighted and dynamic contrast-enhanced MRI of prostate cancer: correlation of quantitative MR parameters with Gleason score and tumor angiogenesis. Am J Roentgenol 197(6):1382–1390
9. Padhani AR, Gapinski CJ, Macvicar DA, et al. (2000) Dynamic contrast enhanced MRI of prostate cancer: correlation with mor-

phology and tumour stage, histological grade and PSA. Clin Radiol 55(2):99–109
10. Isebaert S, De Keyzer F, Haustermans K, et al. (2012) Evaluation of semi-quantitative dynamic contrast-enhanced MRI parameters for prostate cancer in correlation to whole-mount histopathology. Eur J Radiol 81(3):e217–e222
11. Langer DL, van der Kwast TH, Evans AJ, et al. (2010) Prostate tissue composition and MR measurements: investigating the relationships between ADC, T2, K(trans), v(e), and corresponding histologic features. Radiology 255(2):485–494
12. Feldman MK, Gandhi NS (2016) Imaging evaluation of pancreatic cancer. Surg Clin North Am 96(6):1235–1256
13. Sugimoto K, Kim SR, Imoto S, et al. (2015) Characteristics of hypovascular versus hypervascular well-differentiated hepatocellular carcinoma smaller than 2 cm—focus on tumor size, markers and imaging detectability. Dig Dis 33(6):721–727
14. Kusmirek J, Robbins J, Allen H, et al. (2015) PET/CT and MRI in the imaging assessment of cervical cancer. Abdom Imaging 40(7):2486–2511
15. Verma S, Turkbey B, Muradyan N, et al. (2012) Overview of dynamic contrast-enhanced MRI in prostate cancer diagnosis and management. Am J Roentgenol 198(6):1277–1288
16. Loncaster JA, Carrington BM, Sykes JR, et al. (2002) Prediction of radiotherapy outcome using dynamic contrast enhanced MRI of carcinoma of the cervix. Int J Radiat Oncol Biol Phys 54(3):759–767
17. Yamashita Y, Baba T, Baba Y, et al. (2000) Dynamic contrast-enhanced MR imaging of uterine cervical cancer: pharmacokinetic analysis with histopathologic correlation and its importance in predicting the outcome of radiation therapy. Radiology 216(3):803–809
18. Schlaepfer IR, Nambiar DK, Ramteke A, et al. (2015) Hypoxia induces triglycerides accumulation in prostate cancer cells and extracellular vesicles supporting growth and invasiveness following reoxygenation. Oncotarget 6(26):22836–22856
19. Hoskin PJ (2015) Hypoxia dose painting in prostate and cervix cancer. Acta Oncol 54(9):1259–1262
20. Dai Y, Bae K, Siemann DW (2011) Impact of hypoxia on the metastatic potential of human prostate cancer cells. Int J Radiat Oncol Biol Phys 81(2):521–528
21. Hoskin PJ, Carnell DM, Taylor NJ, et al. (2007) Hypoxia in prostate cancer: correlation of BOLD-MRI with pimonidazole immunohistochemistry-initial observations. Int J Radiat Oncol Biol Phys 68(4):1065–1071
22. Chen YJ, Chu WC, Pu YS, et al. (2012) Washout gradient in dynamic contrast-enhanced MRI is associated with tumor aggressiveness of prostate cancer. J Magn Reson Imaging 36(4):912–919
23. Bursac Z, Gauss CH, Williams DK, Hosmer DW (2008) Purposeful selection of variables in logistic regression. Source Code Biol Med 3:17
24. Moran CJ, Hargreaves BA, Saranathan M, et al. (2014) 3D T2-weighted spin echo imaging in the breast. J Magn Reson Imaging 39(2):332–338
25. Kuhl C (2007) The current status of breast MR imaging. Part I. Choice of technique, image interpretation, diagnostic accuracy, and transfer to clinical practice. Radiology 244(2):356–378
26. Tofts PS, Brix G, Buckley DL, et al. (1999) Estimating kinetic parameters from dynamic contrast-enhanced T(1)-weighted MRI of a diffusable tracer: standardized quantities and symbols. J Magn Reson Imaging 10(3):223–232
27. Noworolski SM, Vigneron DB, Chen AP, Kurhanewicz J (2008) Dynamic contrast-enhanced MRI and MR diffusion imaging to distinguish between glandular and stromal prostatic tissues. Magn Reson Imaging 26(8):1071–1080
28. Meyer HJ, Wienke A, Surov A (2018) Correlation between K_{trans} and microvessel density in different tumors: a meta-analysis. Anticancer Res 38:2495–2950
29. Hompland T, Hole KH, Ragnum HB, et al. (2018) Combined MR imaging of oxygen consumption and supple reveals tumor hypoxia and aggressiveness in prostate cancer patients. Cancer Res 78:4774–4785
30. Hambrock T, Somford DM, Huisman HJ, et al. (2011) Relationship between apparent diffusion coefficients at 3.0-T MR imaging and Gleason grade in peripheral zone prostate cancer. Radiology 259(2):453–461
31. Barentsz JO, Richenberg J, Clements R, et al. (2012) ESUR prostate MR guidelines 2012. Eur Radiol 22(4):746–757